Synchrotron-based X-ray spectromicroscopy and electron paramagnetic resonance spectroscopy to investigate the redox properties of lead chromate pigments under the effect of the visible light

Letizia Monico,[1,2,] Koen Janssens,[2] Marine Cotte,[3,4] Aldo Romani,[1] Lorenzo Sorace,[5] Chiara Grazia,[1] Brunetto Giovanni Brunetti,[1] Costanza Miliani.[1]*

[1] CNR Institute of Molecular Science and Technologies (CNR-ISTM) and Centre SMAArt, c/o Department of Chemistry, Biology and Biotechnologies, University of Perugia, via Elce di Sotto 8, 06123 Perugia, Italy.

[2] Department of Chemistry, University of Antwerp, Groenenborgerlaan 171, 2020 Antwerp, Belgium.

[3] European Synchrotron Radiation Facility, Avenue des Martyrs 71, 38000 Grenoble, France.

[4] Laboratoire d'Archéologie Moléculaire et Structurale (LAMS), CNRS-UPMC, UMR 8220, place Jussieu 4, 75005 Paris, France.

[5] Department of Chemistry "U. Schiff" and INSTM RU, University of Florence, Via della Lastruccia 3-13, 50019 Sesto Fiorentino, Italy.

[*] Correspondence: letizia.monico@uantwerpen.be

†Electronic supplementary information (ESI) available.

ABSTRACT

Light-induced redox processes have been established as cause of the chromatic alterations of a number of artists' pigments used from 15th to 20th century.

Despite, the fact that a general comprehension of the mechanisms has been provided through the characterization of the photo-degraded compounds, both exhaustive information on the wavelength-dependence of the alteration process of the pigments and experimental evidences in how the visible light may influence the formation pathways of specific secondary compounds are still lacking.

Establishing an analytical protocol for the study of wavelength-dependence of pigments photo-redox pathways is relevant for a safe illumination of paintings, especially in view of the possible use of spectrally tunable light source such as white light emitting diodes (WLEDs).

In this work, we propose an integrated approach based on a combination of diffuse reflectance UV-Visible, SR-based micro X-ray fluorescence (μ-XRF)/X-ray absorption near edge structure (μ-XANES) and electron paramagnetic resonance (EPR) spectroscopies to study the photo-redox process $Cr(VI) \rightarrow Cr(III)$ for lead chromate yellows ($PbCr_{1-x}S_xO_4$, $0 \leq x \leq 0.8$) under exposure to different monochromatic lights.

In view of the thin (3-5 μm) alteration layer that is formed at the paint surface after light exposure, SR-based Cr K-edge μ-XANES/μ-XRF analysis were employed to obtain information on the abundance, nature and distribution of the alteration of Cr(III)-compounds at the micrometric-scale level. On the other hand, EPR spectroscopy was used as complementary tool to the SR-based X-ray methods due to its sensitivity for revealing species containing one or more unpaired electrons and for distinguishing different coordination geometry of paramagnetic centers, such as Cr(V)-species. Semi-quantitative indications about the darkening of the paint surface were obtained by UV-Vis spectroscopy. An abundance of reduced Cr down to around 50%

was detected at the aged surface of the chrome yellow paints. The reduction process was favored not only by wavelengths shorter than 460 nm (*i.e.,* where the pigment shows its maximum absorption) but also by light in the 490-530 nm range. A first evidence of the presence of Cr(V)-intermediates in the Cr(VI)→Cr(III) reduction reaction allowed the risks of inducing photo-degradation of the 490-530 nm wavelength range to be explained.

1. INTRODUCTION

During the last decades, studies on paint micro-samples taken from original paintings and/or artificially aged model samples have revealed that various pigments, such as vermilion red (HgS),[1,2] realgar/orpiment (yellow-orange arsenic sulfide-based compounds),[3] cadmium yellow (CdS),[4,5,6,7] Prussian blue $(MFe^{III}[Fe^{II}(CN)_6]\cdot xH_2O$, with $M= K^+$, NH_4^+ or $Na^+)$[8,9] and zinc yellow $(K_2O\cdot 4ZnCrO_4\cdot 3H_2O)$,[10] are subject to irreversible chromatic changes as a consequence of redox processes activated by light (sometimes in combination with moisture and/or environmental pollutants).

From a methodological point of view, synchrotron radiation (SR)-based X-ray microprobe techniques, such as micro X-ray fluorescence (μ-XRF), micro X-ray diffraction (μ-XRD) and micro X-ray absorption near edge structure (μ-XANES) methods (in mapping and point analysis mode) have been employed as principal techniques of analysis due to their sensitivity in discriminating between the valence state of the same element and/or in providing information on the distribution of the alteration products within the paint with micrometric spatial resolution.[11,12,13] The capabilities of electron energy loss spectroscopy (EELS) to render additional and/or complementary information at the nanoscale level with respect to the SR-based X-ray methods was also used for studying the distribution and composition of Cr(III)-compounds associated to the degradation of different chromate-based yellows.[14,15] Electrochemical techniques have been proposed as alternative methods for a fast monitoring of the degradation mechanism of a series of photo-degraded semiconductor pigment powders.[16,17]

Despite a general characterization and distribution of the photo-degradation compounds has been established in these studies, neither exhaustive information on the wavelength-dependence of the alteration process of the pigments nor experimental evidences in how different types/doses of the

visible light may influence the pathways of formation of specific secondary compounds have been provided.

Emerging commercial lighting systems, such as white light emitting diodes (WLEDs), have started replacing the more traditional incandescent light sources (such as halogen lamps) over the last few years.[18,19] Among other benefits these devices offer the possibility to illuminate paintings using spectrally tunable lamps.[20,21,22,23]

Thus, defining an analytical procedure for the assessment of the consequences of the visible light on the artists' pigments photo-redox pathways becomes relevant for establishing the appropriate strategies of conservation of irreplaceable masterpieces.

In this work, we propose a multi-method approach based on the combination of diffuse reflectance UV-Vis spectroscopy and metal-speciation methods, such as SR-based μ-XANES/μ-XRF mapping analysis and a X-band (*ca.* 9 GHz) electron paramagnetic resonance (EPR) spectroscopy, for studying the effects of the violet-blue-green light (400-560 nm) and the wavelength-dependence of the redox process in the specific context of chrome yellows ($PbCr_{1-x}S_xO_4$, $0 \leq x \leq 0.8$). Similarly to the above-mentioned pigments, also these compounds are known for their photochemical instability. In particular, our previous studies established that the cause of darkening of chrome yellows in a number of Van Gogh paintings is ascribable to the photo-reduction of the original chromate to Cr(III)-compounds.[24,25] Investigations of aged model paints allowed us to demonstrate that orthorhombic S-rich $PbCr_{1-x}S_xO_4$ ($x \geq 0.5$) compounds show a tendency toward reduction higher than monoclinic S-poor ones ($0 \leq x < 0.4$) and that they degrade upon exposure to violet-blue light (*i.e.,* $400 \leq \lambda \leq 480$ nm).[26,27]

In this paper we employ the above-mentioned analytical protocol to investigate a series of laboratory-prepared chrome yellow paint models ($PbCrO_4/PbCr_{0.2}S_{0.8}O_4$; *i.e.,* with composition similar to the pigments might be found on Van Gogh paintings)[28] that were artificially aged by

employing different commercial white light sources (with different spectral emission in the visible range) and a selection of monochromatic wavelengths. On one hand the combination of diffuse reflectance UV-Vis spectroscopy and SR-based Cr K-edge µ-XANES/µ-XRF mapping analysis were used to obtain information associated with the color change and to determine the amount, nature and distribution of Cr-based alteration compounds within the paints with micrometric resolution. On the other hand EPR spectroscopy was used in a complementary fashion to SR-based X-ray spectromicroscopy methods due to its sensitivity to reveal species containing one or more unpaired electrons and for distinguishing different coordination geometry of paramagnetic centers. As such, it was employed in this work to assess the (possible) presence of Cr(V)-species, that are reported to act as intermediates in the Cr(VI)/Cr(III) photo-reduction process in biological,[29,30,31] catalytic,[32] and polymeric systems.[33,34,35]

2. EXPERIMENTAL

2.1 Preparation of paint models

Paint models (here below denoted as S_{1mono} and S_{3D}) were prepared by mixing $PbCrO_4$ (monoclinic) and $PbCr_{0.2}S_{0.8}O_4$ (mainly orthorhombic) with linseed oil in a mass ratio 4:1 and by applying the mixture on polycarbonate slides. The pigments $PbCrO_4$ (S^*_{1mono}) and $PbCr_{0.2}S_{0.8}O_4$ (S^*_{3D}) were synthesized as described in our previous study.[28]

2.2 Accelerated aging experiments

2.2.1 Spectroradiometric measurements. An irradiance-calibrated AvaSpec-2048-2 spectrometer (Avantes, NL) provided with a 200 μm diameter fiber optic (FC-UVIR200-2-ME, Avantes) and a 8 mm active area cosine corrector (CC-UVVIS/NIR, Avantes) was employed. The spectrometer operates in the 171-1100 nm range (300 lines/mm grating) and is equipped with an AvaBench-75 optical bench, a 25 μm slit which produced 1.2 nm FWHM spectral resolution and a 2048 pixel CCD detector.

Measurements were performed at the samples position using a 5-1000 ms integration time and with 10-50 accumulations. The lamp profiles (Figure 1A) and the corresponding photometric/radiometric quantities (Tables 1-2) were obtained by averaging 20-100 spectral data that were collected throughout the experiment.

2.2.2 Aging with commercial white light sources. Three pc-WLED devices (below indicated as "LED $1_{warm-white}$", "LED $2_{very-warm-white}$", "LED $3_{daylight-white}$"), one halogen lamp and an UV-filtered xenon lamp were used. These systems were selected due to their different emission in the violet-blue-green visible light range, *i.e.,* in the region of maximum absorption of the pigment (Figures 1A-B).

"High-flux" experiments were conducted by keeping illuminance values according to those of Table 1; samples were irradiated for a variable number of hours to obtain an equivalent final

luminous exposure. In order to evaluate any dependence of the degradation process on the photon flux, equivalent aging treatments were also performed under a lower flux regime (here denoted as "low-flux"), with an illuminance approximately decreased by a factor 10^3 (Table 1). The measured temperature close to the sample was around 25-30 °C, with 40-45% relative humidity.

2.2.3. Aging with monochromatic light. A 175 W Cermax xenon lamp equipped with a Horiba Jobin Yvon H10-monochromator (8 nm/mm dispersion and 2 mm slits) was employed for selecting a wavelength range (13-18 nm FWHM; Table 2). A homogenous flux distribution at the sample surface was obtained by placing two lenses up- and down-stream of the monochromator. The IR radiation was minimized using a water filter at the source output.

The wavelengths investigated were chosen on the basis of the absorption profiles of S^*_{1mono} and S^*_{3D} (Figure 1B). Experiments were conducted in the 288-561 nm range, with 4-5 W/m^2 average irradiance and for a variable number of hours to obtain an equivalent number of incident total photon counts (expressed as ph·m^{-2}·nm^{-1}) at end of the aging (Figure 1C and Table 2). Since our previous studies revealed that S_{3D} does not degrade above 570 nm,[27] no experiments at λ>561 nm were performed.

2.3 Methods

2.3.1 UV-Visible. Paints were investigated using a JASCO V-570 spectrophotometer. Diffuse reflectance spectra were recorded in the 200-850-nm range, using a 5 nm spectral bandwidth. The acquisition of unsaturated profiles from a pellet of unaged S^*_{1mono} and S^*_{3D} powders (Figure 1B), prepared by diluting the pigment with $BaSO_4$ in a mass ratio 30:1, were necessary to select the appropriate wavelengths for the monochromatic light aging. The software, interfaced with the instrument, allowed for the conversion of the spectra into CIE L*a*b* chromatic coordinates

under the standard illuminant D65 and 10° angle observer. Total color changes were calculated according to the CIE 1976 formula, $\Delta E^* = (\Delta L^{*2} + \Delta a^{*2} + \Delta b^{*2})^{1/2}$.[36]

2.3.2 SR-based Cr K-edge μ-XANES and μ-XRF. Paints were analyzed in the form of thin sections (about 10 μm in thickness) at the X-ray microscope beamline ID21 of the European Synchrotron Radiation Facility (ESRF, Grenoble, FR).[37]

In order to produce a highly monochromatic primary beam (with $\Delta E/E = 10^{-4}$) a Si (220) fixed-exit double-crystal monochromator was used. The incident beam was focused with Kirkpatrick-Baez mirrors down to a size of 0.8×0.3 μm² (h×v) and maintained stable within 0.5 μm vertical and 0.3 μm horizontal around the Cr K-edge (5.96-6.09 keV).

XRF signals were collected in the horizontal plane and at 69° with respect to the incident beam direction using a single energy-dispersive silicon drift detector (Xflash 5100, Bruker with Moxtek thin polymer window). Two-dimensional μ-XRF maps were obtained *via* raster scanning of the samples by means of the focused X-ray beam and with 100 ms dwell times. Elemental distributions were produced employing the PyMca software.[38] Chemical state maps were obtained by setting the energy of the incoming X-rays at two fixed energy values around the Cr K-edge, where the absorption and consecutively the XRF of particular Cr species are enhanced: (i) at 5.993 keV, for favoring the excitation of the Cr(VI) species, and (ii) at 6.090 keV for collecting XRF signals of all Cr species. The procedure that was used to extract the Cr chemical state distributions is described elsewhere.[26]

One-dimensional series of μ-XANES spectra in XRF mode was perpendicularly collected along the exposed surface of each aged sample; the profiles were obtained by scanning the primary energy across the Cr K-edge with energy increments of 0.2 eV. The ATHENA software[39] was used to perform the normalization and the linear combination fitting of the spectra against a library of XANES profiles of Cr-reference compounds. This procedure allowed for quantitatively

estimating the percentage relative amount of Cr(VI) and Cr(III) species (expressed as $[Cr(VI)]/[Cr_{total}]$ and $[Cr(III)]/[Cr_{total}]$) as a function of the depth.

2.3.3 EPR. X-band EPR spectra of $S*_{3D}$ powder and milled fragments obtained from the pure linseed oil (*i.e.*, not yet mixed with the pigment powders), unaged S_{1mono}/S_{3D} paints and a selection of the corresponding aged materials were recorded using a Bruker E500 continuous-wave spectrometer equipped with a SHQ cavity and for the low temperature spectra, with a continuous flow ^{4}He cryostat (ESR900, Oxford Instruments). g- values were calibrated against a DPPH sample (g=2.0037). Regarding the aged paints, measurements were performed on the material that was selective sampled from the most altered surface.

3. RESULTS AND DISCUSSION

3.1 Exposure to white light sources

3.1.1. Darkening response. In Figures 2A and S1A of the ESI† photographs of the S_{1mono} and S_{3D} paints before and after exposure to different light sources are compared. A color change is appreciable for all the samples, both when exposed to the "high-flux" (Figure 2A) and "low-flux" regimes (Figure S1A†). From the comparison of paint color changes between "high-flux" and "low-flux" experiments kept at similar luminous exposure (Figure 2C and S1B†) it results that the ΔE^* values were rather similar (Table S1†). This result suggests that, within the aging conditions here employed, the lead chromate darkening is not flux-dependent.

The S_{3D} paints show a profound darkening and an alteration layer of about 4-5 μm thickness (Figure 2B). On the other hand and in agreement with our previous studies,[27] the S_{1mono} samples suffer less from darkening. Consistent with these visual observations, UV-Vis spectra show a change of the reflectance in the 510-765 nm range, that progressively decreases with increasing of luminous exposure (see Figure S2† for the spectra collected at "high-flux"). The spectral modifications can be expressed by a decrease in lightness (ΔL^*) and yellowness (Δb^*), that give the major contributions to the total color change (ΔE^*); variations in redness (Δa^*) are smaller (for S_{1mono}) or almost negligible (for S_{3D}) (Figure S3†).

The darkening response of S_{1mono} is similar whatever type of light source is used for aging (Figure 2C): ΔE^* follows a similar trend with luminous exposure and reaches final values of around 7-9. On the contrary, the color change of S_{3D} significantly depends on the type of lighting device: it visibly darkens under the influence of both "LED $1_{warm-white}$" and "LED $3_{daylight-white}$" ($\Delta E^* \sim 30$-31), but not as much as upon exposure to the "halogen" and "UV-filtered xenon" lamps ($\Delta E^* \sim 35$-36). Upon irradiation with "LED $2_{very-warm-white}$", the lowest ΔE^* values are achieved, even though the darkening remains significant ($\Delta E^* \sim 26$).

3.1.2. Cr-speciation investigations. Figures 3A-B show the Cr chemical state maps and the quantitative Cr(VI)/Cr(III) depth profiles obtained *via* linear combination fitting of the Cr K-edge XANES spectra acquired from light-exposed S_{3D} thin sections. The data-sets collected from aged S_{1mono} paints showed slight and similar changes regardless of the aging lamps: a relative amount of Cr(III) not higher than 10-15% was detected at the surface (see Figure S4† for a selection of the XANES profiles). Thus in Figure 3 only the results obtained from the aged S_{3D} samples are presented.

Regarding the "high-flux" experiments, S_{3D} paints exposed either to LED $1_{warm-white}$" or "LED $3_{daylight-white}$" (Figures 3A1,3) show the presence of a superficial Cr(III)-rich layer of 3-4 μm in thickness, while Cr(VI)-species are the main constituents of the yellow paint underneath. A similar distribution can be observed after aging with the "halogen" and the "UV-filtered xenon" lamps (Figures 3A4,5). The sample irradiated using "LED $2_{very-warm-white}$" (Figure 3A2) reveals the presence of Cr(III)-species at the surface as well, but in lower amount than in other paints.

One-dimensional series of Cr K-edge XANES spectra, collected from the cross-sectioned S_{3D} samples *vs.* depth below the expose surface confirm the reduction of the original Cr(VI) (Figure S5†); this is demonstrated by a decrease of the Cr pre-edge peak intensity at 5.993 keV and the shift of the absorption edge toward lower energies.[26,27] These changes are more pronounced in the spectra collected in the upper 1-3 μm of the thin sections and after aging with the "halogen" and "UV-filtered xenon" lamps (Figures S5D-E†).

In line with our previous studies,[27] three fitting components, such as $PbCr_{0.2}S_{0.8}O_4$, Cr (III)-oxides [*i.e.,* $Cr(OH)_3/Cr_2O_3$] and either Cr(III) acetate [$(CH_3CO_2)_7Cr_3(OH)_2$], Cr(III) acetylacetonate [$Cr(C_5H_7O_2)_3$], or $Cr_2(SO_4)_3 \cdot H_2O$ were necessary to obtain a good description of the XANES spectra recorded along the first 1-3 μm of each sample (see Table S2† for details about the fitting results). Only two components [$PbCr_{0.2}S_{0.8}O_4$ plus one from the three species:

Cr (III)-oxides/Cr(III)-organo-metal compounds/$Cr_2(SO_4)_3 \cdot H_2O$] were required to fit the profiles recorded at greater depth. It is worth to underline that regardless of which components were used, the fitting models yielded comparable [Cr(III)]/[Cr_{total}] ratio (Table S2†).

The average Cr(III)-amount at the surface decreases when going from the paints aged either with "halogen" or "UV-filtered xenon" lamps ($\approx$55%) to that irradiated with "LED 2 $_{\text{very-warm-white}}$" ($\approx$30%) (Figures 3B2 and 4-5, light-red and green lines/dots; Table S2†). Its abundance was about 35% after exposure to "LED 1$_{\text{warm-white}}$" and "LED 3$_{\text{daylight-white}}$" (Figures 3B1,3; Table S2†). For all samples, the average Cr(III)-amount progressively decreases with increasing of depth down to values of about 10%.

After "low-flux" aging, the Cr(VI)/Cr(III) depth profiles (Figure 3B1-4, dark-red and green lines/dots) show a similar trend as obtained after "high-flux" experiments, but with a lower average Cr(III)-amount at the surface (about 20-25%; Table S2†).

A positive correlation between the ΔE^* and the average Cr(III)-amount at the paint surface (upper first µm) is observable in Figure 3C, suggesting that, under our aging conditions, UV-Vis measurements may provide an indirect information on the amount of photo-reduction of Cr(VI) in S_{3D}.

Interestingly, the photo-response of S_{3D} toward different lamps cannot be justified by only taking into account their total photon counts in the range of maximum absorption of S_{3D} (*i.e.*, 400-460 nm, in the Vis range) (*cf.* Figures 1B and S6†). "LED 1$_{\text{warm-white}}$" and "LED 3$_{\text{daylight-white}}$" yielded comparable levels of darkening, despite "LED 1$_{\text{warm-white}}$" shows a lower total emission than "LED 3$_{\text{daylight-white}}$" in the range 400-460 nm. Similarly, the significant effect of the halogen lamp on the reduction process (*i.e.,* comparable to that of the "UV-filtered xenon" device) cannot be explained on the basis of its emission profile in the 400-460 nm range. This observation suggests that also other wavelength bands of the visible light might activate the darkening process. This

aspect is explored in more detail in the following section by discussing the results obtained from S_{3D} and S_{1mono} paints that were aged using a selection of wavelengths in the UV-Vis region.

3.2 Exposure to monochromatic light

In Figure 4A, the photographs of S_{1mono} and S_{3D} paints after exposure to different wavelengths are shown. At the naked eye a darkening is visible for all paints; it becomes progressively less significant for aging wavelengths above 500 nm. These qualitative observations were confirmed by UV-Vis spectroscopy: in the 500-765 nm range, the profiles show a decrease of reflectance to a different extent with increasing of incident photon counts (Figure S7†). These changes can be expressed by a decrease both in L^* and b^* (both representing the largest contribution to ΔE^*); the observed differences in a^* were small (Figure S8†).

In Figures 4B-C, the ΔE^* values recorded during the exposure of S_{3D} and S_{1mono} to different wavelengths are plotted *vs.* the incident photon counts. The darkening of S_{1mono} (Figure 4C), both at 400 and 500 nm is less significant than the equivalent ones obtained from S_{3D} (Figure 4B, dark-green and purple line/dots). S_{1mono} darkens more strongly upon exposure at 500 nm rather than at 400 nm, reaching a $\Delta E^*_{500\ nm}$ of about 4-5 ($\Delta E^*_{400\ nm} \approx 2$).

The darkening of S_{3D} decreases with increasing wavelength (Figure 4B). The most significant color change ($\Delta E^* \approx 16\text{-}17$) is observable after exposure at 288 nm. The ΔE^* decreases to about 11-12 for the paint irradiated at 400 nm and to about 8 for that exposed at 450 nm. A smaller but still appreciable ΔE^* (≈ 4) is observable after aging at 531 nm, while it is negligible (≈ 2) upon exposure at 561 nm. Notably, the result obtained at 500 nm is out of this trend: the $\Delta E^*_{500\ nm}$ changes in a way similar to that observed at 400 nm.

Figures 5A-B shows the quantitative Cr(VI)/Cr(III) depth profiles and a selection of the Cr chemical state maps obtained from S_{3D} paints aged by means of monochromatic light (Table S3†). The Cr(III)-amount decreases with increasing depth (down to 5-10%) and its different

values at the surface depend on the employed aging wavelength. After exposure at 288 nm, the formation of a superficial 5 µm thick layer composed of 45-50% of Cr(III) is observed (Figures 5A1 and 5B, on top). Cr(III)-species in amount of about 25% and 20% were also found within the upper 5 µm of the samples aged at 400 and 450 nm, respectively (Figure 5A2-3). The exposure at 500 and 531 nm gave rise to the formation of a 2-3 µm thick superficial layer, that contains about 20% of Cr(III)-compounds (Figures 5A4-5 and 5B, on bottom). Within the upper 13 µm depth of the sample aged at 561 nm (Figure 5A6), these alteration products are present in abundance of about 13-15% (Table S3†).

The plot ΔE^* values *vs.* the Cr(III)-amount (averaged at the first µm paint surface) is shown in Figure 5C where a quite complex correlation is observable. Two different positive correlations are visible: one for the samples aged at 288, 400 and 450 nm (Figure 5C, black-dotted line) and the other for those exposed at $\lambda \geq 500$ nm (red-dotted line). The result suggests that upon exposure to different wavelengths, a number of degradation pathways might take place; these can promote the formation of various Cr(III)-based compounds with different UV-Vis absorption properties. Within the limits of the data treatment procedure, this hypothesis is also supported by the fitting results of the XANES spectra (Table S3†): these suggest that Cr(III)-oxides are more likely formed at the surface (upper 1-2 µm) of the samples aged at 288, 400 and 500 nm, while Cr(III)-organo-metal compounds in those irradiated at 450, 531 and 561 nm.

The efficiency of both 500 and 400 nm radiation to induce darkening/Cr reduction can provide an explanation for the S_{3D} response toward exposure to different commercial light sources, including that of the "LED $1_{warm\text{-}white}$" and "halogen" lamps (see Section 3.1.2). As Figure 6 illustrates, this is indicated by the positive correlation between the average Cr(III)-amount at the surface and the total photon counts in the 385-415 nm and 485-515 nm range (*cf.* Figure S6† for the emission profiles of light sources expressed as photon counts).

The efficiency of the alteration process at 500-530 nm wavelength (expected to be much smaller than at λ<450 nm, considering the low absorption of the pigment in this region; *cf.* Figure 1B) could be justified taking into account that other Cr-species [*e.g.,* Cr(IV) or Cr(V) complexes] are characterized by an absorption in this spectral range and might be formed as a result of a reaction between the original chromate and the polymeric matrix.[31,33-35,40,41] Under light exposure these species can act as intermediates in the reduction process.

A first attempt aimed at evaluating the possible presence of other reduced paramagnetic Cr-species is presented in the next section, where the results obtained by EPR measurements both on unaged S_{1mono}/S_{3D} paints and a selection of the corresponding aged materials are reported.

3.3 EPR investigations

Preliminary EPR analyses were performed on the S^{*}_{3D} powder and the pure linseed oil. In agreement with the diamagnetic character of the Cr(VI)-ion, the pigment did not show any relevant EPR signal (spectrum not reported). A temperature-dependent spectrum (Figure S9A†) is observed for the organic binder, with a signal shifting from 2540 Oe (g=2.65) at room temperature to 1240 Oe (g=5.42) at 5 K. This signal is attributable to cobalt, manganese or iron polynuclear mixed valence clusters. As reported in the literature,[42] compounds of these transition metals are likely to have been used as oil driers. In particular, the shift in resonance field suggests the formation of superparamagnetic aggregates.[43]

The spectra of the unaged S_{3D} and S_{1mono} paints (Figure 7, leftmost panel) evidence the presence of several signals of different nature in the 1000-5000 Oe field range. Of particular interest is the structured band with two narrow components (Figure 7, rightmost panel) observed at g=1.987 [resonance field (H_{res})=3551 Oe] and g=1.9804 (H_{res}=3561 Oe). Their position, their relatively small width (ΔH_{pp}~10 Oe) and the possibility to easily observe them at room temperature are consistent with the presence of Cr(V)-centers.[29-31,44] The observation of two different resonance

fields, more evident for S_{1mono}, might be explained either by considering the formation of two different Cr(V)-based species or to a weak g-anisotropy of the formed species.[30-32]

A broad band, centered at approximately g=2.0, is also evident in both samples. Its width ($\Delta H_{pp} \sim 650$ Oe) and the absence of characteristic features makes it difficult to provide a definitive assignment. However, since the observation of Cr(V) in both unaged paints indicates that the mixing of the powder with the binder triggers a redox reaction involving Cr(VI), it is plausible to assign these signals to Cr(III)-based compounds, *e.g.,* Cr(III)-sulfate (Figure S9B†) or Cr(III)-oxide.[45] For $S_{3D,}$ an additional signal at half field (g=4.00) is observed: this is consistent with the presence of Cr(III)-species; nevertheless, other S>1/2 paramagnetic species could contribute to it.[46]

The EPR spectra of the aged paints (Figure 7, "S_{1mono}/S_{3D}-UV filtered xenon", "S_{3D}-LED 1$_{warm-white}$") show features similar to those observed for the unaged ones (broad resonance centered close to g=2.0 [Cr(III)-species], half field transition (g=4.0) for "S_{3D}-LED 1$_{warm-white}$", narrow signal at g=1.979 [Cr(V)-species]). However, an additional narrow signal at g=1.999 is present (Figure 7, rightmost panel). Based on its g-value this is ascribable to the formation of an organic radical or of an electronic vacancy within the lattice upon irradiation. In the "S_{3D}-UV filtered xenon" and "S_{3D}-LED 1$_{warm-white}$" spectra, the relative intensity of the broad band at g=2.0 compared to the narrow one at g=1.979 is higher than in the un-aged samples. In line with the above-discussed XANES data, this result indicates an increase of the Cr(III)-amount after aging.

The persistence of Cr(V)-species in the aged paints can be explained by taking into account that EPR measurements we conducted on bulk samples. Although a selective sampling of the most altered surface of paints was performed, a residual portion of the yellow bulk material underneath may contribute to the observed signals. However, it should not be excluded that Cr(V) is also produced as a primary species during the Cr(VI)/Cr(III) photoreduction.[34,35] This

would also explain the difference in the effective g values for the Cr(V)-signals attributed in aged (g=1.979) and un-aged (g=1.987) samples.

As the literature reports,[30,31] Cr(V)-compounds are generally unstable at room temperature; thus, so far they have been never been included in the XANES fitting model (Tables S2-3† and refs. 25-27). Nevertheless, since Cr(V)-materials show a pre-edge peak at around 5.992 keV [*i.e.,* slightly shifted toward lower energy relative to that of Cr(VI) species (5.993 keV)] and with an intensity higher than that of Cr(III)-compounds,[31] these fits may have resulted in a (slight) over-estimation of the Cr(VI)-abundance. A combined EPR/SR-based X-ray study on the formation/reduction of Cr(V)-species is foreseen for the next future.

CONCLUSIONS

In this work, an integrated approach based on the combination of diffuse reflectance UV-Vis, SR µ-XANES/µ-XRF and EPR spectroscopies was successfully used to study the redox properties of different chrome yellow varieties (PbCrO$_4$, PbCr$_{0.2}$S$_{0.8}$O$_4$) under effect of the visible light and different monochromatic lights. While diffuse reflectance UV-Vis measurements allows to determine which wavelengths are most readily absorbed and what color-alteration effects these have, the SR-based micro-techniques are most useful to extract information from the micrometric thin upper layer of altered material, without interference from the original unaltered paint mass, (still) present below the degradation layer. Since the SR-based methods are used on materials that have been subject to degradation conditions for relative long period of time, EPR is employed complementarily to these, considering it allows to detect the formation of transient degradation-species even though it does not provide laterally resolved information.

Our observations indicate that wavelengths below 460 nm and at around 500 nm are the most active in stimulating the reduction of Cr(VI) to Cr(III)-compounds and that thermally formed Cr(V)-species act as intermediates of the Cr(VI)/Cr(III) redox process.

In particular, after exposure to different commercial white light sources, SR µ-XANES/µ-XRF and diffuse reflectance UV-Vis measurements revealed that the abundance of Cr(III)-compounds localized at the outer surface (upper 1-2 µm) correlated with the degree of paint darkening and that the process is not (strongly) radiant flux-dependent. PbCrO$_4$ paints (denoted as S$_{1mono}$) showed up to 10-15% of Cr(III)-amounts, irrespective of the illumination device employed. On the contrary, the Cr(III)-abundance in PbCr$_{0.2}$S$_{0.8}$O$_4$ samples (denoted as S$_{3D}$) gradually increased with increasing of amount of the violet-blue radiations (*i.e.*, around the maximum absorption region of the pigment) and of the green light (500-530 nm) emitted by the white sources, ranging from about 25% to 55%. The sensitivity of this pigment in both spectral ranges was

unequivocally confirmed by similar investigations carried out on a series of $PbCr_{0.2}S_{0.8}O_4$ paints exposed to a selection of monochromatic lights.

The efficiency of the green radiation to induce the alteration process could be explained *via* EPR identification of Cr(V)-compounds, that may absorb radiation in this spectral range. Depending on the aging wavelengths, we suggest that these intermediates may play a key role in driving the photo-reduction of Cr(VI)-species toward the formation of different Cr(III)-compounds.

The information gained from this study indicates that the exposure to the violet-blue-green radiation (400-530 nm) should be minimized as much as possible for the safe display of paintings containing chrome yellows.

The multi-technique approach here proposed in combination with monochromatic photochemical aging could be used for assessing the redox proprieties of other pigments under effect of the visible light. In particular, EPR spectroscopy, is expected to find a wider applicability in the context of artist's pigment degradation studies, since its suitability as laboratory technique in providing complementary/additional metal-speciation information to SR-based X-ray spectromicroscopic methods.

FIGURES

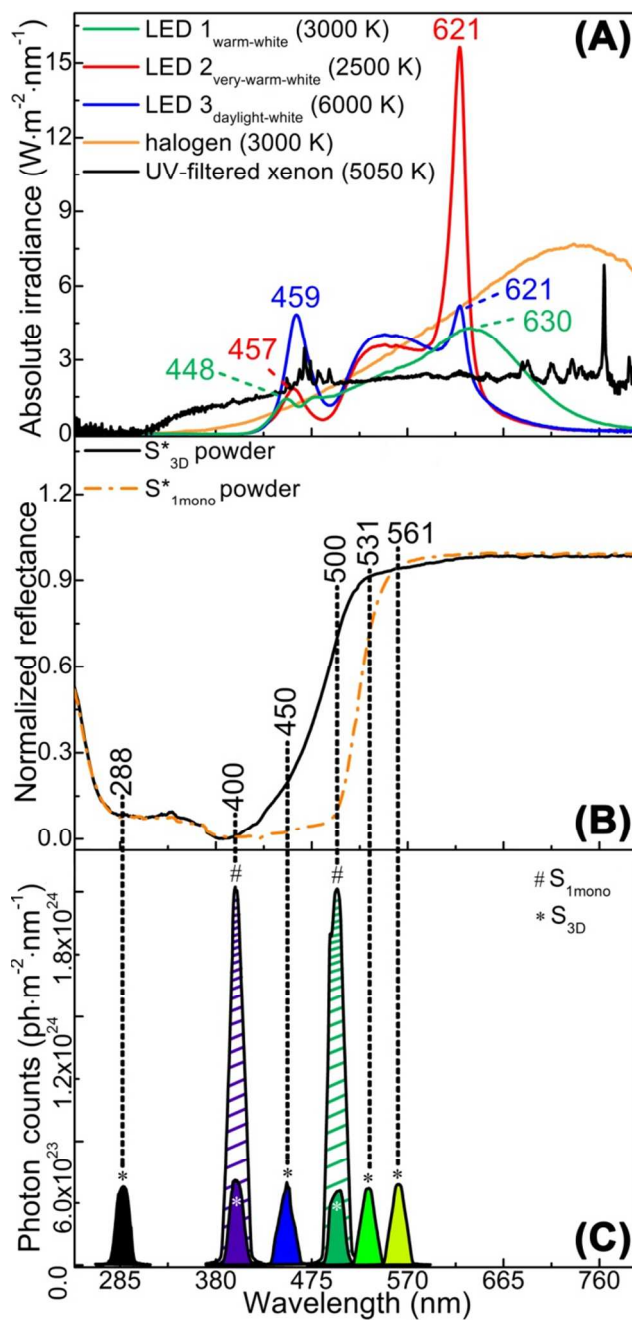**Figure 1.** (A) Irradiance profiles of the lamps used for the aging of $PbCrO_4$ (S_{1mono}) and $PbCr_{0.2}S_{0.8}O_4$ (S_{3D}) paints. (B) Diffuse reflectance UV-Vis spectra of (black) S^*_{3D} and (orange) S^*_{1mono} powders. (C) Profiles of the wavelength ranges employed for monochromatic light aging of (asterisk) S_{3D} and (hash) S_{1mono} (see Tables 1-2 for details).
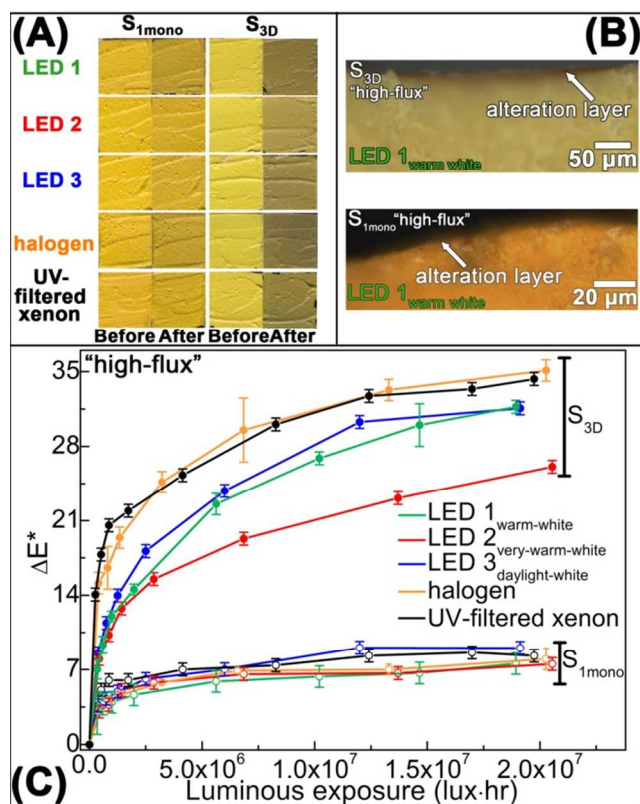
Figure 2. (A) Photographs of S_{3D} and S_{1mono} paints before and after "high-flux" exposure to different lamps. (B) Microphotograph of (top) S_{3D} and (bottom) S_{1mono} thin sections aged using "LED $1_{warm-white}$" at "high-flux". (C) Plot of ΔE^* *vs.* the luminous exposure acquired during "high-flux" experiments of (filled circles) S_{3D} and (empty circles) S_{1mono} (see Figures S2-3 of the ESI† for the corresponding UV-Vis spectra and plot of ΔL^*, Δa^*, Δb^* *vs.* the luminous exposure).
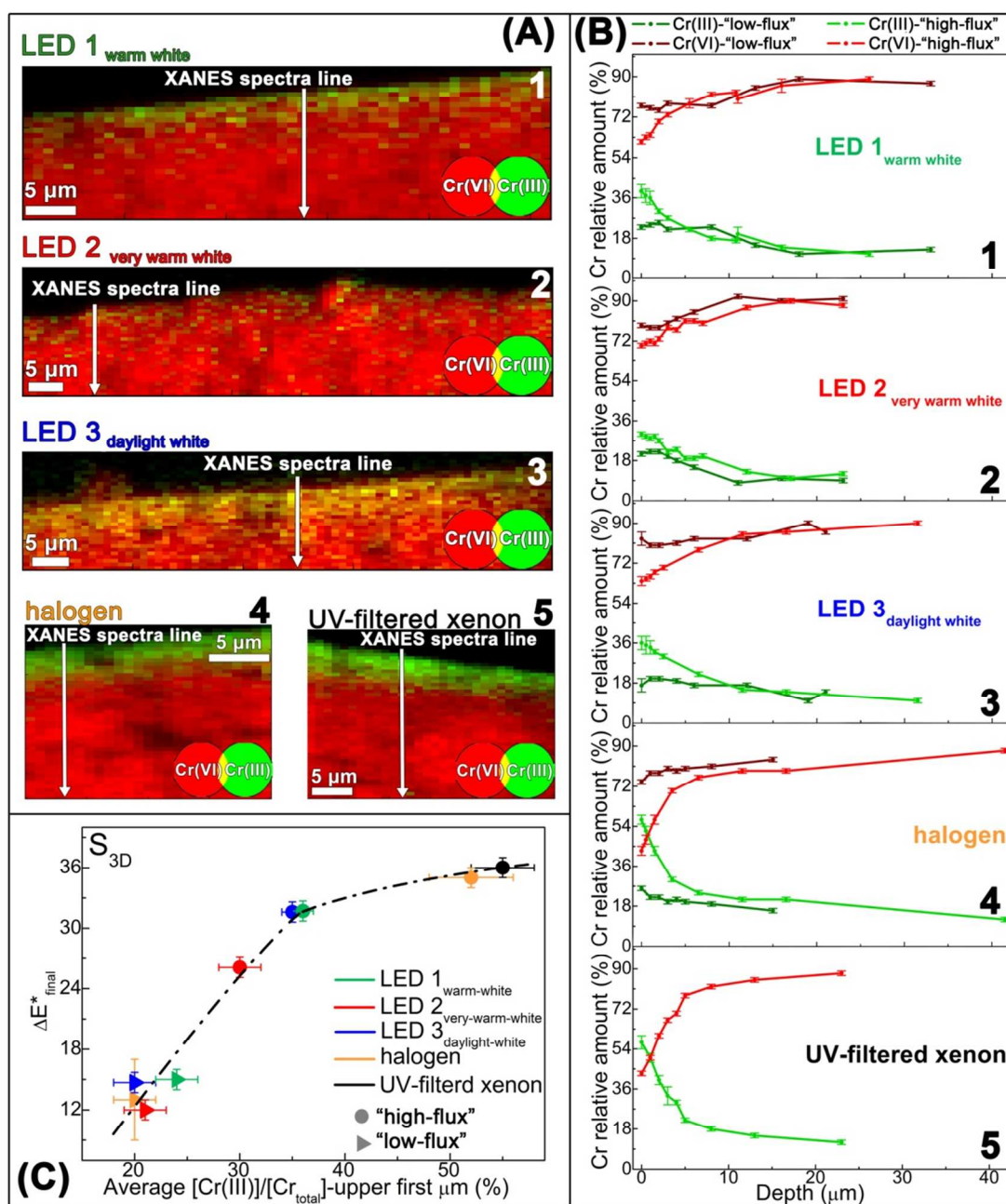
Figure 3. (A) RG Cr(VI)/Cr(III) chemical state maps obtained from S_{3D} after "high-flux" exposure to different lamps [step sizes (h×v): $0.8×0.3$ μm^2; dwell time: 100 ms/pixel]. (B) Quantitative Cr(III)/Cr(VI) depth profiles, obtained as a linear combination fitting of different Cr-reference compounds to the line of XANES spectra recorded from the "high-flux" and "low-flux" aged S_{3D} paints (see Figure S4-5 and Table S2 of the ESI† for the XANES profiles and the fit results). For the "high-flux" experiments the regions of XANES analysis are indicated in (A1-5). (C) Plot of ΔE^*_{final} vs. the average Cr(III) relative amount of the upper first micrometer.
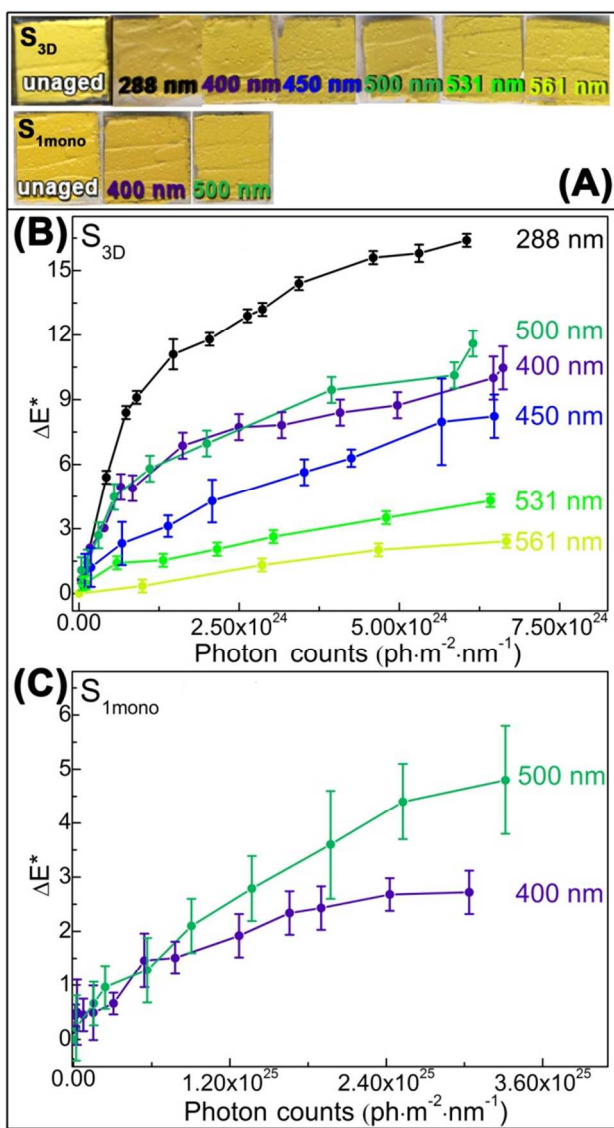
Figure 4. (A) Photographs of (top) S_{3D} and (bottom) S_{1mono} paints before and after monochromatic light aging (Table 2). Plot of ΔE^* *vs.* incident photon counts at different wavelengths for (B) S_{3D} and (C) S_{1mono} (see Figures S7-8 of the ESI† for the corresponding UV-Vis spectra and plot of ΔL^*, Δa^*, Δb^* *vs.* incident photon counts).
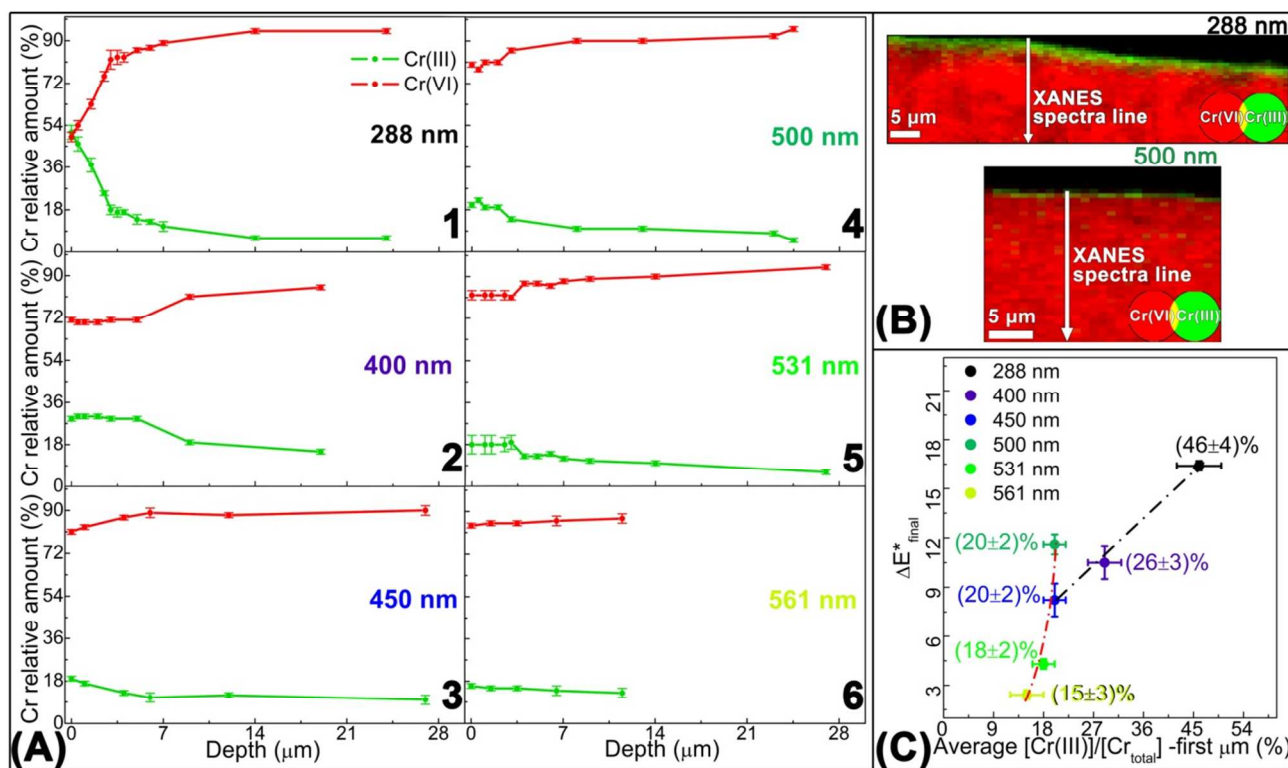
Figure 5. (A) Quantitative Cr(III)/Cr(VI) depth profiles, obtained as a linear combination fitting of different Cr-reference compounds to the line of XANES spectra acquired from the monochromatic light aged S_{3D} paints [see Table S3† for the fitting results]. (B) RG Cr(VI)/Cr(III) chemical state maps obtained from S_{3D} paints after exposure at 288 nm and 500 nm [step sizes (h×v): 0.8×0.3 μm²; dwell time: 100 ms/pixel]. (D) Plot of ΔE*$_{final}$ *vs.* the average Cr(III) relative amount of the upper first micrometer.
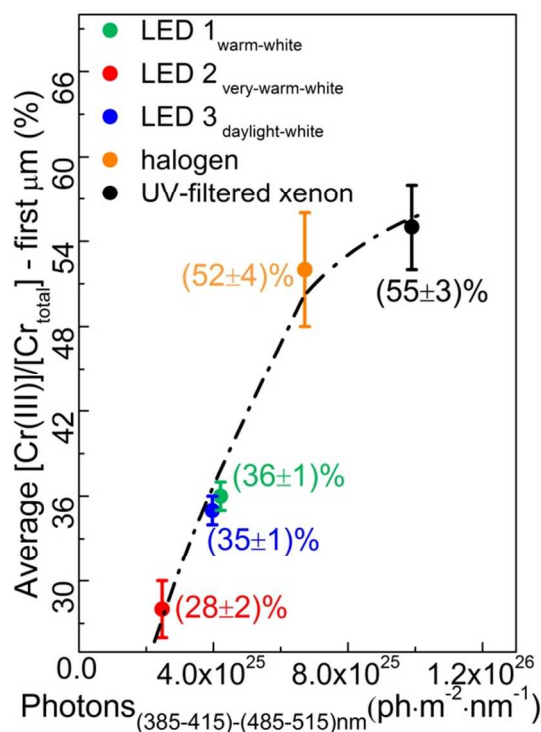
Figure 6. Plot of the average Cr(III) percentage relative amount of the upper first micrometer *vs.* the sum of the photon counts in the 385-415 nm and 485-515 nm range (*cf.* Figure S6 and Table S2 of the ESI†).

Figure 7. Room temperature EPR spectra of S_{1mono} (grey) and S_{3D} (black) paints before (upper) and after (lower) aging. Leftmost panel shows the full spectral range while the rightmost one illustrates a magnification of the g = 2.00 region.

TABLES

Table 1. Experimental conditions used for the aging of chrome yellow model paints using different commercial lamps.
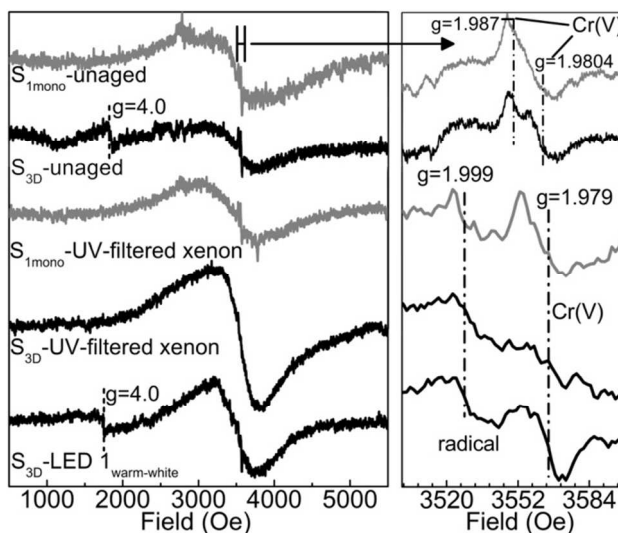
Lighting devices[a]	Correlated color temperature (K)	Illuminance (lux)	Aging time (hrs)[b]
LED 1 warm-white	3000	2.0×10^5 (high-flux)	~96
		1.1×10^3 (low-flux)	~745
LED 2 very-warm-white	2500	2.85×10^5 (high-flux)	~72
		6×10^2 (low-flux)	~745
LED 3 daylight-white	6000	2.5×10^5 (high-flux)	~76
		5.5×10^2 (low-flux)	~745
halogen	3000	2.7×10^5 (high-flux)	~76
		6×10^2 (low-flux)	~745
UV-filtered xenon	5050	1.72×10^5 (high-flux)	~114

[a] CRI/$R_a \geq 85$. [b]According to CIE recommendations[36] limiting annual exposure for oil paintings in a museum are about 600 klux·hours/year; thus, paints were irradiated for *ca.* 30 years ("high-flux") and 7-13 years ("low-flux").

Table 2. Experimental conditions used for the monochromatic light aging of chrome yellow model paints.

Sample*	Wavelength (nm)	FWHM (nm)	Irradiance (W·m^{-2})	Total photon counts	Aging time (hrs)
S$_{3D}$ (mainly orthorhombic PbCr$_{0.2}$S$_{0.8}$O$_4$)	288	15	4.5±0.2	6.04×10^{24}	~254
	400	16	4.8±0.5	6.62×10^{24}	~190
	450	13	3.8±0.2	6.5×10^{24}	~212
	500	17	4.5±0.4	6.04×10^{24}	~150
	531	16	3.7±0.1	6.4×10^{24}	~180
	561	17	3.9±0.2	6.7×10^{24}	~180
S$_{1mono}$ (monoclinic PbCrO$_4$)	400	16	4.3±0.1	3.04×10^{25}	~967
	500	18	5.3±0.1	3.04×10^{25}	~694

*See ref. 28 for additional details about the molecular and structural properties of each sample.

NOTES AND REFERENCES

1 M. Radepont, W. de Nolf, K. Janssens, G. Van der Snickt, Y. Coquinot, L. Klaassen and M. Cotte, *J. Anal. Atom. Spectrom.*, 2011, **26**, 959-968.

2 M. Radepont, Y. Coquinot, K. Janssens, J. J. Ezrati, W. de Nolf and M. Cotte, *J. Anal. Atom. Spectrom.*, 2015, **30**, 599-612.

3 K. Keune, J. Mass, F. Meirer, C. Pottasch, A. van Loon, A. Hull, J. Church, E. Pouyet, M. Cotte and A. Mehta, *J. Anal. Atom. Spectrom.*, 2015, **30**, 813-827.

4 G. Van der Snickt, J. Dik, M. Cotte, K. Janssens, J. Jaroszewicz, W. De Nolf, J. Groenewegen and L. van der Loeff, *Anal. Chem.,* 2009, **7**, 2600-2610.

5 G. Van der Snickt, K. Janssens, J. Dik, W. De Nolf, F. Vanmeert, J. Jaroszewicz, M. Cotte, G. Falkenberg and L. van der Loeff, *Anal. Chem.*, 2012, **84**, 10221-10228.

6 J. L. Mass, R. Opila, B. Buckley, M. Cotte, J. Church and A. Mehta, *Appl. Phys. A: Mater. Sci. Process.*, 2013, **111**, 59-68.

7 J. Mass, J. Sedlmair, C. S. Patterson, D. Carson, B. Buckley and C. Hirschmugl, *Analyst*, 2013, **138**, 6032-6043.

8 L. Samain, F. Grandjean, G. J. Long, P. Martinetto, P. Bordet, J. Sanyova and D. Strivay, *Synchrotron Radiat.* 2013, **20**, 460-473.

9 L. Samain, G. Silversmit, J. Sanyova, B. Vekemans, H. Salomon, B. Gilbert, F. Grandjean, G. J. Long, R. P. Hermann, L. Vincze and D. Strivay, *J. Anal. Atom. Spectrom.* 2011, **26**, 930-941.

10 L. Zanella, F. Casadio, K. A. Gray, R. Warta, Q. Ma and J. F. Gaillard, *J. Anal. Atom. Spectrom.*, 2011, **26**, 1090-1097.

11 L. Bertrand, L. Robinet, M. Thoury, K. Janssens, S. X. Cohen and S. Schöder, *Appl. Phys. A: Mater. Sci. Process*, 2012, **106**, 377-396.

12 K. Janssens, M. Alfeld, G. Van der Snickt, W. De Nolf, F. Vanmeert, L. Monico, S. Legrand, J. Dik, M. Cotte, G. Falkenberg, L. van der Loeff, M. Leeuwestein and E. Hendriks, in *Science and Art: the Painted Surface*, ed. A. Sgamellotti, B. G. Brunetti and C. Miliani, Royal Society of Chemistry, London, 2014, ch. 18, pp. 373-403.

13 M. Cotte, J. Susini, J. Dik and K. Janssens, *Acc. Chem. Res.*, 2010, **43**, 705-714.

14 F. Casadio, S. Xie, S. C. Rukes, B. Myers, K. A. Gray, R. Warta and I. Fiedler, *Anal. Bioanal. Chem.*, 2011, **399**, 2909-2920.

15 H. Tan, H. Tian, J. Verbeeck, L. Monico, K. Janssens and G. Van Tendeloo, *Angew. Chem. Int. Edit.*, 2013, **52**, 11360-11363.

16 W. Anaf, S. Trashin, O. Schalm, D. van Dorp, K. Janssens and K. De Wael, *Anal. Chem.* 2014, **86**, 9742-9748.

17 W. Anaf, K. Janssens and K. De Wael, *Angew. Chem. Int. Edit.* 2013, **125**, 12800-12803.

18 J. Padfield, S. Vandyke and D. Carr, http://www.nationalgallery.org.uk/paintings/research/improving-our-environment, (accessed March 2015).

19 K. Matsushima, T. Nishimura, S. Ichikawa, M. Sekiguchi, T. Tanaka, A. Hakata and F. Tazuke, *J. Light & Vis. Env.*, 2010, **34**, 195-210.

20 A. Tuzikas, A. Žukauskas, R. Vaicekauksas, A. Petrulis, P. Vitta and M. Shur, *Opt. Express*, 2014, **22**, 16802-16818.

21 R. S. Berns, *Color Res. Appl.*, 2011, **36**, 324-334.

22 F. Viénot, G. Coron and B. Lavédrine, *J. Cult. Herit.*, 2011, **12**, 431-440.

23 M. F. Delgado, C. W. Dirk, J. Druzik and N. WestFall, *Color Res. Appl.*, 2011, **36**, 238-254.

24 L. Monico, G. Van der Snickt, K. Janssens, W. De Nolf, C. Miliani, J. Dik, M. Radepont, E. Hendriks, M. Geldof and M. Cotte, *Anal. Chem.*, 2011, **83**, 1224-1231.

25 L. Monico, L. K. Janssens, F. Vanmeert, M. Cotte, B. G. Brunetti, G. Van der Snickt, M. Leeuwestein, J. Salvant Plisson, M. Menu and C. Miliani, *Anal. Chem.* 2014, **86**, 10804-10811.

26 L. Monico, G. Van der Snickt, K. Janssens, W. De Nolf, C. Miliani, J. Verbeeck, H. Tian, H. Tan, J. Dik, M. Radepont and M. Cotte, *Anal. Chem.*, 2011, **83**, 1214-1223.

27 L. Monico, K. Janssens, C. Miliani, G. Van der Snickt, B. G. Brunetti, M. Cestelli Guidi, M. Radepont and M. Cotte, *Anal. Chem.*, 2013, **85**, 860-867.

28 L. Monico, K. Janssens, C. Miliani, B. G. Brunetti, M. Vagnini, F. Vanmeert, G. Falkenberg, A. Abakumov, Y. Lu, H. Tian, J. Verbeeck, M. Radepont, M. Cotte, E. Hendriks, M. Geldof, L. van der Loeff, J. Salvant and M. Menu, *Anal. Chem.*, 2013, **85**, 851-859.

29 J. A. Howe, R. H. Loeppert, V. J. DeRose, D. B. Hunter and P. M. Bertsch, *Environ. Sci. Technol.*, 2003, **37**, 4091-4097.

30 A. Levina, H. H. Harris and P. A. Lay, *J. Am. Chem. Soc.*, 2007, **129**, 1065-1075.

31 A. Levina, L. Zhang and P. A. Lay, *Inorg. Chem.*, 2003, **42**, 767-784.

32 B. M. Weckhuysen, L. M. De Ridder, P. J. Grobet and R. A. Schoonheydt, *J. Phys. Chem.-US*, 1995, **99**, 320-326.

33 A. Berger, L. Frezet and Y. Israëli, *J. Phys. Chem. B*, 2009, **113**, 14218-14224.

34 G. Manivannan, R. Changkakoti, R. A. Lessard, G. Mailhot and M. Bolte, *J. Phys. Chem. B*, 1993, **97**, 7228-7233.

35 C. Pizzocaro, C. Lafond and M. Bolte, *J. Photoch. Photobio. A*, 2002, **151**, 221-228.

36 Commission Internationale de L'Eclairage, *Control of damage to museum objects by optical radiation*, CIE 157:2004, ISBN: 3901906274.

37 M. Salomé, M. Cotte, R. Baker, R. Barrett, N. Benseny-Cases, G. Berruyer, D. Bugnazet, H. Castillo-Michel, C. Cornu, B. Fayard, E. Gagliardini, R. Hino, J. Morse, E. Papillon, E. Pouyet, C. Rivard, V. A. Solé, J. Susini and G. Veronesi, *J. Phys.: Conf. Ser.*, 2013, **425**, 182004.

38 V. A. Solé, E. Papillon, M. Cotte, P. Walter and J. Susini, *Spectrochim. Acta B*, 2007, **62**, 63–68.

39 B. Ravel and M. J. Newville, *Synchrotron Radiat.*, 2005, **12**, 537–541.

40 B. M. Weckhuysen, L. M. De Ridder and R. A. Schoonheydt, *J. Phys. Chem.-US*, 1993, **97**, 4756-4763.

41 R. Codd, P. A. Lay and A. Levina, *Inorg. Chem.* 1997, **36**, 5440-5448.

42 F. Miccichè, M. A. van Straten, W. Minga, E. Oostveen, J. van Haveren, R. van der Linde and J. Reedijk, *Int. J. Mass Spectr.* 2005, **246**, 80–83.

43 M. Fittipaldi, L. Sorace, A. L. Barra, C. Sangregorio, R. Sessoli and D. Gatteschi, *Phys. Chem. Chem. Phys.,* 2009, **11**, 6555–6568.

44 B. M. Weckhuysen, I. E. Wachs and R. A. Schoonheydt, *Chem. Rev.*, 1996, **96**, 3327-3350.

45 A. Bruckner, *Chem. Commun.* 2001, **20**, 2122–2123.

46 J. R. Pilbrow, *Transition Ion Electron Paramagnetic Resonance,* Clarendon Press, Oxford, 1991.

An integrated approach based on UV-Visible, SR µ-XRF/µ-XANES and EPR spectroscopies is proposed as protocol to study the redox properties of chrome yellows under exposure to visible and monochromatic lights.